17th World Congress on Computational Mechanics (WCCM)
10th European Congress on Computational Methods in Applied Sciences and Engineering (ECCOMAS)
19 - 24 July 2026, Munich, Germany

ON THE EVALUATION OF SPATIAL AND TEMPORAL NUMERICAL DISSIPATION IN INCOMPRESSIBLE FLOWS

SARA-MEDINA ŠEHOVIĆ[1], JOSEP PLANA-RIU[1], F. XAVIER TRIAS[1] AND ASSENSI OLIVA[1]

[1] Heat and Mass Transfer Technological Center (CTTC)
Technical University of Catalonia (UPC), ESEIAAT
Carrer de Colom 11, 08222 Terrassa (Barcelona), Spain
e-mail: sara.medina.sehovic@upc.edu

Key words: Energy budgets, Energy conservation, Numerical and physical dissipation, Spatial and temporal discretization, Symmetric operators, Global and local energy budgets.

Summary. *This work proposes a framework for the evaluation of spatial and temporal errors in incompressible flows, which aims to help distinguish the physical dissipation of the fluid from numerical, artificial dissipation of a numerical simulation. Spatial discretization of the governing equations often breaks the symmetry that is present in their balancing continuous operators, causing energy dissipation in a fluid even in cases where the set-up states that the energy must be physically conserved. Furthermore, temporal integration schemes are well-known to be a cause of artificial dissipation in Computational Fluid Dynamics (CFD) simulations. Higher-order temporal discretization schemes tend to reduce the numerical dissipation. However, they require high computational costs, which further underlines the need for efficient tools for numerical dissipation quantification.*

Hence, these problems require an approach that would help us identify sources of numerical dissipation in CFD simulations, with the aim to verify the simulation, improve the accuracy and reduce the computational effort. This work presents an approach that allows for the identification and quantification of artificial dissipation in simulations, running on traditional test cases such as Rayleigh–Taylor instability in buoyancy–driven flows, and channel flow, based on following the energy budgets of the flow. Furthermore, it helps detect configuration issues in simulation setup, as well as check the accuracy of the underlying operators and interpolators used in a simulation.

1 INTRODUCTION

The fundamental goal of Computational Fluid Dynamics (CFD) is to solve discrete governing equations as accurately as possible, but at the lowest computational cost. Over the decades, various discretization schemes were developed, both for spatial and the temporal discretization of governing equations. Additionally, distinguishing physical energy dissipation from artificial numerical damping remains a major challenge in CFD. As demonstrated by Verstappen [1], controlling non-linear numerical instabilities requires a rigorous balance of dissipation, reinforcing

the need to isolate physical, subgrid-scale, and artificial numerical contributions. However, various discretized operators do not adhere to the symmetry of their corresponding differential operators. Consequently, such discretization schemes do not preserve the energy-conserving properties of the continuous governing equations. This creates artificial dissipation, which can significantly interfere with real, physical dissipation of the fluid. In their paper, Verstappen and Veldman [2] emphasized the importance of energy preservation in CFD simulations and demonstrated a discretization method that preserves the symmetric properties of the operators, which was later extended to a collocated framework by Trias et al. [3].

Temporal discretization schemes are well-known to cause artificial dissipation. Temporal errors are highly dependent on the order of discretization and time-step size conditions. Achieving high accuracy temporal discretization schemes requires high computational effort. In their works Capuano et al. [4] and Sanderse [5], systematically investigated how standard multi-stage time-integration methods introduce temporal energy errors in incompressible flows, demonstrating that energy conservation is only achieved by means of symplectic (implicit) time-integration schemes, though improved properties can be obtained in explicit integrators if a pseudosymplectic formulation is used.

In large eddy simulations (LES), an additional problem arises; the numerical dissipation is often hidden in subgrid scale model dissipation. Because of this, it is crucial to distinguish between the physical, model and numerical dissipation.

For the reasons explained above, it was found crucial to develop a method that would allow us to diagnose and quantify discretization errors. Traditionally, energy budgets have been used in CFD simulations almost exclusively as a post-processing tool for understanding the flow physics. Recently, work was done by Komen et al. [6], who introduced a novel quantification method to evaluate numerical dissipation in quasi-DNS and under-resolved DNS by leveraging these dissipation balances. Building on this rationale, rather than using the energy budgets solely to observe fluid physics, our approach leverages fully discrete kinetic energy budgets as a diagnostic tool to explicitly identify, isolate, and quantify artificial dissipation introduced by spatial operator discretizations and temporal time-stepping schemes. The spatial discretization errors are identified by the global vs. local approach, calculating the energy budgets in the system as a global, and at each control volume, respectively. Ideally, these two approaches should exactly coincide, and any observed difference indicates artificial numerical dissipation. The temporal errors were monitored in multi-step and multi-stage integration schemes.

This paper explains the theoretical background of the problem presented, which consists of the governing equations, the matrix-vector notation, energy-conserving formulation, and evaluation of global and local energy budgets, as well as evaluation of spatial and temporal integration schemes. The results outline the observed cases, the Rayleigh–Taylor instability in buoyancy-driven flow, and channel flow are presented.

2 GOVERNING EQUATIONS

The governing Navier–Stokes (NS) equations, for incompressible Newtonian flows with constant physical properties are given as:

$$\nabla \cdot \boldsymbol{u} = 0, \tag{1}$$

$$\rho \frac{\partial \boldsymbol{u}}{\partial t} + \rho(\boldsymbol{u} \cdot \nabla)\boldsymbol{u} = -\nabla p + \mu \nabla^2 \boldsymbol{u} + \boldsymbol{S}, \tag{2}$$

which represent the conservation of mass and momentum, respectively. The total kinetic energy of the system for $\rho = 1$ is defined as:

$$E_k = \int_\Omega \frac{1}{2} u^2 dV = \frac{1}{2} \langle \boldsymbol{u}, \boldsymbol{u} \rangle = \frac{1}{2} \|\boldsymbol{u}\|^2 \in \mathbb{R}, \tag{3}$$

where $\langle \boldsymbol{a}, \boldsymbol{b} \rangle = \int_\Omega \boldsymbol{a} \cdot \boldsymbol{b} \, \mathrm{d}V$ is the inner-product of two functions. Similarly, by taking the inner product of the velocity $\boldsymbol{u}$ and the momentum equation given in Eq. (2), as follows:

$$\frac{dE_k}{dt} = \frac{1}{2} \frac{d\langle \boldsymbol{u}, \boldsymbol{u} \rangle}{dt} = \left\langle \boldsymbol{u}, \frac{\partial \boldsymbol{u}}{\partial t} \right\rangle = -\langle \boldsymbol{u}, C(\boldsymbol{u}, \boldsymbol{u}) \rangle + \nu \langle \boldsymbol{u}, \nabla^2 \boldsymbol{u} \rangle - \langle \boldsymbol{u}, \nabla p \rangle, \tag{4}$$

we obtain the global balance equation for total kinetic energy E_k. Here, $C(\boldsymbol{u}, \boldsymbol{u}) = (\boldsymbol{u} \cdot \nabla)\boldsymbol{u}$ is the convective term and $\nu = \mu/\rho$. Applying Gauss's divergence theorem under boundary conditions with no boundary contributions, the surface integrals vanish. Additionally, for incompressible flows, $\nabla \cdot \boldsymbol{u} = 0$, Eq. (4) becomes:

$$\frac{dE_k}{dt} = -\nu \langle \nabla \boldsymbol{u}, \nabla \boldsymbol{u} \rangle = -\nu ||\nabla \boldsymbol{u}||^2. \tag{5}$$

As presented above, in the absence of a source term and contributions from the domain's boundary, $\partial\Omega$, the total kinetic energy $E_k(t)$ will decrease due to the effect of the viscous dissipation.

2.1 Matrix-vector notation

The semi-discrete, spatially-discretized NS equations are read as:

$$M \boldsymbol{u}_s = \boldsymbol{0}_c, \tag{6}$$

$$\Omega \frac{d\boldsymbol{u}_c}{dt} + C(\boldsymbol{u}_s)\boldsymbol{u}_c = D\boldsymbol{u}_c - \Omega G_c \boldsymbol{p}_c + \boldsymbol{f}_c. \tag{7}$$

Here, $\boldsymbol{u}_c = (\boldsymbol{u}_1, \boldsymbol{u}_2, \boldsymbol{u}_3)^T \in \mathbb{R}^{3n}$ is the collocated (cell-centered) vector that contains the three spatial components of the velocity, and $\boldsymbol{u}_s$ is the staggered velocity vector at the cell faces. The relationship between the collocated and staggered velocities is $\boldsymbol{u}_s = \Gamma_{c \to s} \boldsymbol{u}_c \in \mathbb{R}^m$, where $\Gamma_{c \to s} \in \mathbb{R}^{m \times 3n}$ is a cell-to-face interpolator. Then, $C(\boldsymbol{u}_s) \in \mathbb{R}^{3n \times 3n}$ and $D \in \mathbb{R}^{3n \times 3n}$ are

the discrete convective and diffusive terms in integral form, respectively, while $M \in \mathbb{R}^{n\times m}$ represent the divergence operator in the integral form. $G_c \in \mathbb{R}^{3n\times n}$ is the discrete gradient, and $\Omega \in \mathbb{R}^{3n\times 3n}$ is a diagonal matrix containing the cell volumes. The subscripts c and s denote cell-centered and face-staggered variables, respectively. Notice that n is the number of cells whereas m is the number of faces.

From the Eq. (3), we can see the definition of the total kinetic energy of the system. Similarly, we can define the total kinetic energy at discrete level as:

$$E_k = \frac{1}{2}\boldsymbol{u}_c^T \Omega \boldsymbol{u}_c. \tag{8}$$

Finally, we can derive the kinetic energy equation in the matrix-vector form by taking the inner-product of the discrete velocity field $\boldsymbol{u}_c$ and the momentum equation given in Eq (7):

$$\frac{dE_k}{dt} = -\boldsymbol{u}_c^T C(\boldsymbol{u_s})\boldsymbol{u}_c + \boldsymbol{u}_c^T D\boldsymbol{u}_c - \boldsymbol{u}_c^T \Omega G_c \boldsymbol{p}_c + \boldsymbol{u}_c^T \boldsymbol{f}_c. \tag{9}$$

3 ENERGY-CONSERVING FORMULATION

As explained before and shown in Eq. (4), in the absence of source terms and contributions from the domain's boundary, the kinetic energy of the system will decrease due to the viscous dissipation. Relying on the analogy of continuous and discrete operators, the same can be derived for the latter. Therefore, in the absence of external forces or contributions from the domain boundary, we obtain:

$$\frac{dE_k}{dt} = \boldsymbol{u}_c^T D\boldsymbol{u}_c \leq 0. \tag{10}$$

To ensure that the discrete NS equations respect the same physical conservation laws as the continuous system, the discrete operators must preserve the structural properties of corresponding differential operators. According to [2], this is achieved by defining the convective operator $C(\boldsymbol{u}_s)$ as skew-symmetric, and the diffusive operator $D = \nu(I_3 \otimes L)$ as symmetric negative-definite where $L = MG \in R^{n\times n}$ is the Laplacian, and $I_3 \in \mathbb{R}^{3\times 3}$ the identity matrix, $G \in \mathbb{R}^{m\times n}$ component-wise cell-to-face discrete gradient. In summary, discrete operators have to fulfill the following requirements:

- **Convective operator:** Skew-symmetric - $C = -C^T$
- **Diffusive operator:** Symmetric negative definite - $D = D^T < 0$
- **Gradient and divergence operators:** Negative adjoints - $M^T = -\Omega_s G$

4 EVALUATION OF NUMERICAL DISSIPATION

4.1 Evaluating spatial discretization errors

The evaluation of discretization error follows the approach of calculating the energy budgets at the global and local levels. The global approach treats the energy budgets in the system as

a whole, while the local approach calculates the energy budgets at each control volume. In an ideal case, the energies calculated at the global and local levels should coincide, otherwise demonstrating the artificial dissipation, as calculating the system's total energy should be equal to the sum of energies at each control volume.

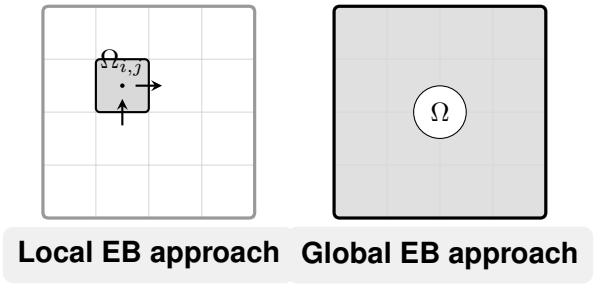

Figure 1: Global vs. Local approach

The viscous dissipation, crucial for detecting the artificial dissipation due to the nature of its operators, as given in Eqs. (5) and (10), is calculated differently depending on the global vs. local approach. The calculation of the dissipative term for the constant viscosity field, in the global approach is calculated as:

$$\left.\frac{dE_k}{dt}\right|_{dissipative} = \boldsymbol{u}_c^T D \boldsymbol{u}_c. \tag{11}$$

The calculation of the viscous term in the local approach is done as:

$$\left.\frac{dE_k}{dt}\right|_{dissipative} = -\nu \mathbf{1}_c^T \Pi_{c\to s}^T \sum_{k=1}^{3} \Omega_s \left(G\boldsymbol{u}_k\right) \odot \left(G\boldsymbol{u}_k\right), \tag{12}$$

where $\Pi_{c\to s}^T \in \mathbb{R}^{n\times m}$ is the transposed cell-to-face interpolator, $\boldsymbol{u}_k \in \mathbb{R}^n$ represents the k-th spatial velocity component, $\mathbf{1}_c^T \in \mathbb{R}^n$ is a cell-centered vector of ones, $\Omega_s \in \mathbb{R}^{m\times m}$ is the diagonal matrix of face-centered control volumes, and $\odot$ denotes the Hadamard (element-wise) product. Hence, the energy budgets of the total volume should coincide with the sum at the control-volume level. Comparing the two approaches should ideally yield the same results. Any discrepancy between the two approaches, the global approach and the total sum of local contributions, points to the spatial numerical dissipation.

4.2 Evaluating temporal discretization errors

Numerical errors have been observed in multi-step and multi-stage time-integration methods. The approach consists in calculating the energy budgets for a constant time step $\Delta t = const.$ at the mid-step $t^{n+1/2}$, and calculating the exact energy budget formulation for the corresponding time-integration scheme. The scope of this work deals with the temporal discretization errors in multi-step and multi-stage time-integration schemes.

For a constant time step Δt, the energy budgets are calculated at $t^{n+1/2}$ as

$$\left.\frac{\mathrm{d}E_k}{\mathrm{d}t}\right|^{n+1/2} = \left(-\boldsymbol{u}_c^T C(\boldsymbol{u}_s)\boldsymbol{u}_c + \boldsymbol{u}_c^T D\boldsymbol{u}_c - \boldsymbol{u}_c^T \Omega G_c \boldsymbol{p}_c + \boldsymbol{u}_c^T \boldsymbol{f}_c\right)^{n+1/2}. \tag{13}$$

To evaluate discrete temporal energy conservation, we define the momentum equations in terms of the right-hand side operator $\boldsymbol{R}$, defined as:

$$\boldsymbol{R} \equiv -\Omega^{-1} C(\boldsymbol{u}_s)\boldsymbol{u}_c + \Omega^{-1} D\boldsymbol{u}_c - G_c \boldsymbol{p}_c + \boldsymbol{f}_c. \tag{14}$$

For multi-step time-integration schemes (e.g. Adams–Bashforth methods), the energy budgets are calculated as:

$$\frac{E_k^{n+1/2+\kappa} - E_k^{n-1/2+\kappa}}{\Delta t} = (\boldsymbol{u}_c^{n+\kappa})^T \Omega \boldsymbol{R}(\tilde{\boldsymbol{u}}_c^{n+\kappa}), \tag{15}$$

where $\tilde{\boldsymbol{u}}_c^{n+\kappa} \equiv (1+\kappa)\boldsymbol{u}_c^n - \kappa \boldsymbol{u}_c^{n-1}$ and κ is the scheme parameter (e.g. $\kappa = 1/2$ for a second-order Adams–Bashforth scheme).

On the other hand, for multi-stage time-integration schemes (such as Runge-Kutta methods), the energy budgets are calculated as:

$$\frac{E_k^{n+1} - E_k^n}{\Delta t} = \left(\frac{\boldsymbol{u}_c^{n+1} + \boldsymbol{u}_c^n}{2}\right)^T \Omega \left(\sum_{i=1}^{s} b_i \boldsymbol{R}(\boldsymbol{U}_i)\right), \tag{16}$$

where s is the number of stages, b_i are the quadrature weights of the Runge–Kutta scheme, and $\boldsymbol{U}_i \in \mathbb{R}^{3n}$ denotes the intermediate stage velocity vector for stage i ($i = 1, \ldots, s$). Similarly, for a perfectly conservative time-integration scheme, the two approaches to calculate energy budgets in time should coincide. The difference between the approaches quantifies the numerical error caused by temporal discretization. Furthermore, this approach serves as a tool to compare a simulation set-up for different time-integration schemes and helps choose the most optimal one.

5 NUMERICAL TESTS

Numerical tests in this work were performed using the in-house code TermoFluids Algebraic (TFA), with underlying algebraic kernels implemented in the HPC^2 framework [7] . The operations were performed based on the matrix-vector formulation, mirroring the approach explained in previous sections. The Rayleigh–Taylor case was chosen for the Direct Numerical Simulation (DNS) numerical test, while the channel flow case was chosen for the LES test.

5.1 Rayleigh–Taylor instability

The first numerical experiment was performed for the Rayleigh–Taylor instability case. The configuration of the case consisted of a rectangular domain of aspect ratio $A = 2$, filled with a

fluid at cold temperature at the top and hot temperature at the bottom. Cold fluid represents the "heavy" fluid, while the hot fluid is the "light" fluid, causing the fluid movement. Following the approach by Sanderse and Trias (2024) [8], a small perturbation is added to the hot and cold fluid interface, defined as $y = 1.0 + 0.05\sin(2\pi x)$. The fluid was set at Prandtl number $Pr = 0.71$, Rayleigh number $Ra = 10^6$ and Gebhart number $Ge = 1$. The domain boundaries are adiabatic ($\frac{\partial T}{\partial n} = 0$) and no-slip $\boldsymbol{u} = 0$. The mesh used was 128×256.

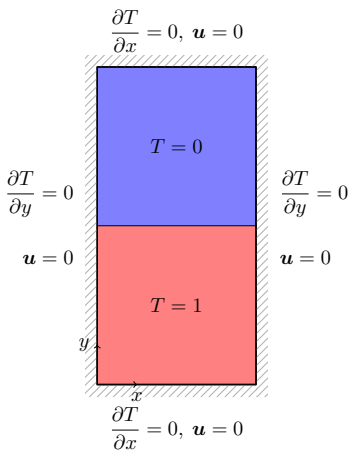

(a) Rayleigh–Taylor domain setup

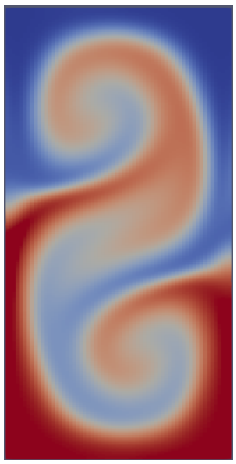

(b) Rayleigh–Taylor flow instantaneous field

Figure 2: Rayleigh–Taylor problem setup and instability flow visual.

Time evolution of kinetic, potential, and internal energy budgets gave useful insight into the physical meaning of the fluid motion. In buoyancy-driven flows, with no sources and contributions from the boundaries, such as is the case in the Rayleigh–Taylor case, the energy converts from one type to another, merely, from potential to kinetic, and then from kinetic to thermal (internal) energy and similar.

$$Potential\ energy\ \Rightarrow Kinetic\ energy\ \Rightarrow Thermal\ (internal)\ energy$$

Mathematically, the flow must satisfy the following condition:

$$\frac{dE_{kinetic}}{dt} + \frac{dE_{potential}}{dt} + \frac{dE_{internal}}{dt} = 0. \tag{17}$$

As mentioned above, the Rayleigh–Taylor case in buoyancy-driven flows was chosen as it represents a convenient way to test the Eq. (17), considering that the potential energy of the system should be converted into kinetic energy, driven by the buoyancy forces, and finally, it is dissipated into internal energy of the system. The adiabatic boundary walls ensure no contributions from the boundaries. The resulting energy budget evaluations are presented below.

Figure 3 shows the time evolution of kinetic energy budgets, i.e. rate of change of energy in our Rayleigh–Taylor buoyancy driven flow, from the initial conditions until reaching the steady

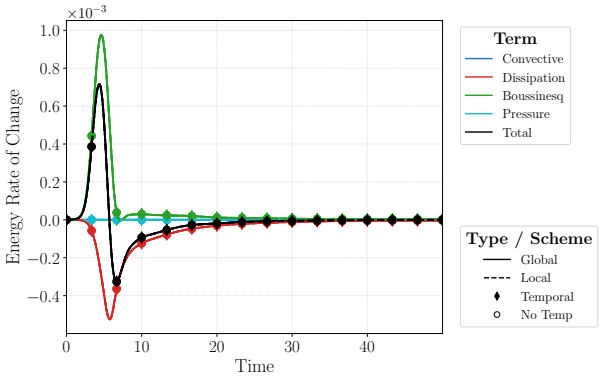

Figure 3: Energy budgets for Rayleigh–Taylor flow at $Ra = 10^6$ and $Ge = 1$ ($A = 2,\ 128 \times 256$)

state. It can be seen that the energy driver of the system is the buoyancy force. Then, this energy is converted into dissipative (internal) energy. On the plot, we can see that in the steady state, the total rate of change of kinetic energy goes to zero, meaning that the system reaches an equilibrium.

On the other hand, Figure 4 represents the behavior of the rate of change of energy of the potential, kinetic and internal energy. According to Eq. (17), the total change in a closed, buoyancy-driven system should be zero. Here, we can see that in the Rayleigh–Taylor flow, the total rate of change of energy follows Eq. (17).

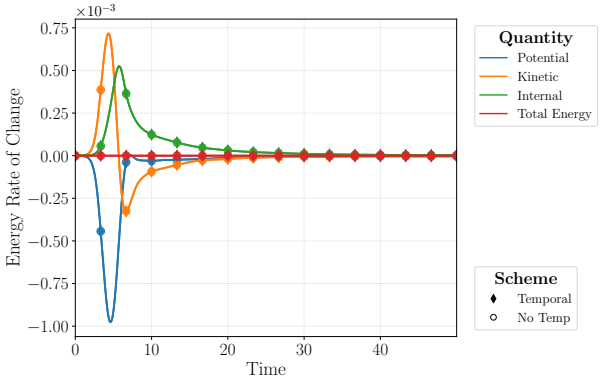

Figure 4: Rate of change of kinetic, potential, and internal energies for the Rayleigh–Taylor flow ($Ra = 10^6,\ Ge = 1, A = 2,\ 128 \times 256$)

Finally, we present the results of time evolution of kinetic, potential and internal energy budgets of a Rayleigh–Taylor case in Figure 5. The reference potential energy at the initial time step $t = 0$ is set to be $E_p = 0$. As predicted, the potential energy of the fluid is converted into kinetic by buoyancy forces. Then, this energy is converted into internal energy by dissipative forces. The reason why potential energy is negative is because, as mentioned, the reference

potential energy is considered $E_p = 0$. The hot and cold fluids keep mixing until the equilibrium is reached. It can be seen from Figure 5 that after reaching the steady state, the potential energy of the system is fully converted into internal energy. Additionally, total energy of the system was observed,

$$E_{kinetic} + E_{potential} + E_{internal} = 0. \tag{18}$$

From here, we can see that the total energy was constantly ≈ 0. It was calculated that the average difference, from the Eq. 18 was $\times 10^{-11}$, which is two orders lower than the solver accuracy of 10^{-9}.

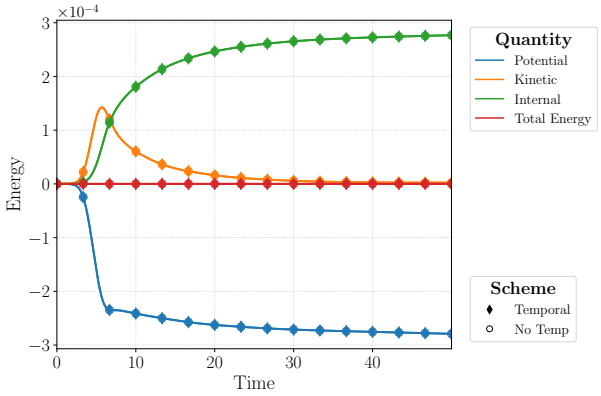

Figure 5: Time evolution of kinetic, potential, and internal energy budgets for the Rayleigh–Taylor flow ($Ra = 10^6,\ Ge = 1, A = 2,\ 128 \times 256$)

5.2 Channel flow

The second test was performed for an LES simulation of turbulent channel flow. Based on the benchmark case by Kim et al. [9], the computational domain has size $(L_x, L_y, L_z) = (4\pi\delta, 2\delta, 2\pi\delta)$ in the streamwise (x), wall-normal (y), and spanwise (z) directions, respectively, with periodic boundary conditions applied in the streamwise and spanwise directions, and channel half-width δ. The friction Reynolds number is $Re_\tau = 180$, and no-slip conditions ($\boldsymbol{u} = 0$) are imposed on the top and bottom solid walls. A grid of $32 \times 32 \times 32$ cells was used. The flow is driven by a constant mean pressure gradient $\partial p/\partial x = 1.0$ to maintain a constant mass flow rate. Grid nodes are stretched in the wall-normal direction using a hyperbolic tangent function [10], $y_i = \delta \left(1 + \tanh\left(\gamma\left(\frac{2i}{N_y} - 1\right)\right) / \tanh\gamma\right)$ for $i = 0, 1, \ldots, N_y$, with stretching parameter $\gamma = 2.0$ and channel half-width δ, ensuring adequate resolution of both the viscous sublayer and outer-layer energy budgets. Time integration is performed using a second-order Adams–Bashforth scheme ($\kappa = 1/2$). The subgrid-scale eddy viscosity ν_{sgs} was modeled using the WALE formulation [10].

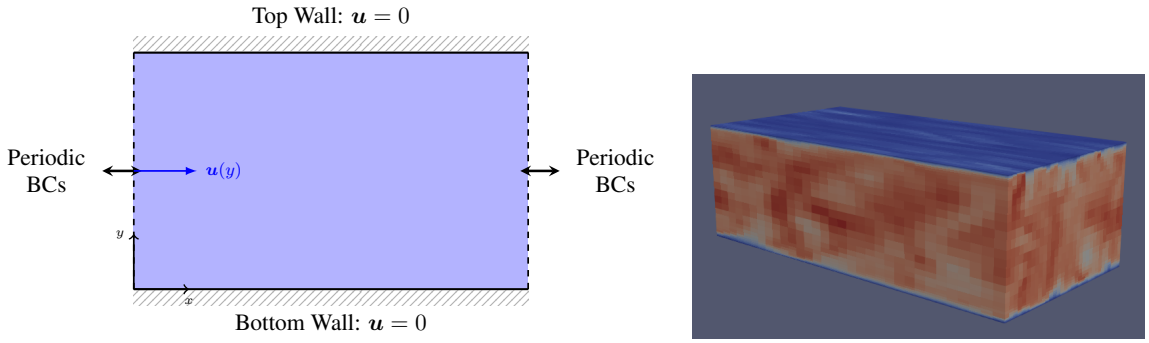

(a) Channel flow domain setup

(b) Channel flow instantaneous field

Figure 6: Channel flow problem setup and instantaneous velocity field.

5.3 LES simulation & numerical dissipation

The governing NS equations for LES simulations in matrix-vector form are given as:

$$M\overline{\boldsymbol{u}}_s = \mathbf{0}_c, \tag{19}$$

$$\Omega\frac{\mathrm{d}\overline{\boldsymbol{u}}_c}{\mathrm{d}t} + C(\overline{\boldsymbol{u}}_s)\overline{\boldsymbol{u}}_c = D\overline{\boldsymbol{u}}_c + D_{\mathrm{SGS}}(\nu_{\mathrm{sgs}})\overline{\boldsymbol{u}}_c - \Omega G_c\overline{\boldsymbol{p}}_c + \overline{\boldsymbol{f}}_c, \tag{20}$$

where a spatial filtering operation (with filter width $\bar{\Delta}$) is applied to the governing equations to separate the velocity field $\boldsymbol{u}$ into a resolved scale component $\overline{\boldsymbol{u}}$ and an unresolved subgrid-scale (SGS) component $\boldsymbol{u}'$.

Unlike DNS simulations, which exhibit physical and numerical dissipation, in LES simulation, the total dissipation has physical, numerical and sub-grid scale (SGS) contributions:

$$\varepsilon_{total} = \varepsilon_{physical} + \varepsilon_{SGS\ model} + \varepsilon_{numerical\ dissipation}. \tag{21}$$

Hence, in addition to the DNS Rayleigh–Taylor case, we have to solve the energy budgets of the SGS model:

$$\frac{\mathrm{d}\overline{E}_k}{\mathrm{d}t} = \overline{\boldsymbol{u}}_c^T D\overline{\boldsymbol{u}}_c + \overline{\boldsymbol{u}}_c^T D_{\mathrm{SGS}}(\nu_{\mathrm{sgs}})\overline{\boldsymbol{u}}_c = -\varepsilon_{\mathrm{physical}} - \varepsilon_{\mathrm{SGS}}. \tag{22}$$

Figure 7 represents the time evolution of rate of change of kinetic energy budgets in the channel flow LES simulation at $Re_\tau = 180$. Here, it can be seen that at the beginning, the kinetic energies are changing rapidly. Later on, the flow reaches a statistically stationary state. In this equilibrium regime, the time-averaged total rate of change of kinetic energy approaches zero ($\langle dE_k/dt \rangle \approx 0$), confirming that energy production by the driving mean pressure gradient ($\partial p/\partial x = -1.0$) balances the total dissipation ($\varepsilon_{\mathrm{total}} = \varepsilon_{\mathrm{physical}} + \varepsilon_{\mathrm{SGS}}$). The total rate of change is dominated by the SGS model and viscous fluid dissipation during the initial transient phase.

This confirms that for the chosen mesh ($32 \times 32 \times 32$) and second-order Adams–Bashforth time step, the numerical dissipation introduced by temporal time-stepping remains minimal relative to the physical and subgrid-scale dissipation mechanisms.

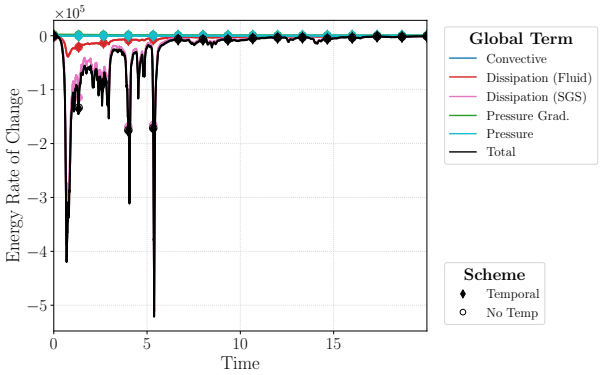

Figure 7: Energy Budgets in Channel Flow case using LES model ($Re_\tau = 180,\ 32 \times 32 \times 32$)

6 CONCLUSIONS

This work deals with the development of a systematic tool which allows for detection and quantification of numerical errors. It was shown that preserving the symmetry of discrete operators, like the skew-symmetry and negative adjointness is crucial for elimination of non-physical energy contributions. Another important note in following the energy budgets of a simulation is to successfully distinguish between spatial and temporal discretization errors. By implementing the approach of calculating the energy at global and local level, it was possible to evaluate and compare numerical dissipation in a simulation. It was proven to be a rigorous framework for validating time-step selection and SGS models in complex flows. Through continuous and discrete energy budget balances, the proposed global versus local formulation serves as a rigorous verification tool:

- DNS Rayleigh–Taylor Instability: The total system energy conservation condition ($E_{\text{kinetic}} + E_{\text{potential}} + E_{\text{internal}} = 0$) was satisfied to an accuracy of $\mathcal{O}(10^{-11})$, two orders of magnitude below the iterative solver tolerance (10^{-9}), demonstrating complete absence of spurious spatial dissipation.

- LES Turbulent Channel Flow: The framework successfully disentangled physical viscous dissipation ($\varepsilon_{\text{physical}}$) and subgrid-scale model dissipation (ε_{SGS}) from numerical integration errors, providing clear diagnostics during both transient and steady-state turbulence.

Evaluating the discrete temporal residuals enables direct comparison of multi-step (Adams–Bashforth) schemes, offering a sound physical criterion for optimal time-step selection. Future work will focus on extending this diagnostic framework to unstructured complex geometries, leveraging the temporal energy residual as a feedback signal for adaptive time-stepping algorithms, and applying the formulation to variable-density scalar transport. Additionally, it will focus on comparison between the multi-step and multi-stage time-integration schemes.

7 ACKNOWLEDGMENTS

S.M.Š. is supported by MULTITHERM II project (PID2023-153281OB-I00) of *Ministerio de Ciencia, Innovación y Universidades*, Spain. J.P-R., F.X.T. and A.O. are supported by SIMEX project (PID2022-142174OB-I00) of *Ministerio de Economía y Competitividad*, Spain.

REFERENCES

[1] R.W.C.P. Verstappen. How much dissipation is needed to restrain numerical instabilities? *Computers & Fluids*, Vol. 176, pp. 276–284, 2018.

[2] R.W.C.P. Verstappen and A.E.P. Veldman. Symmetry-preserving discretization of turbulent flow. *Journal of Computational Physics*, Vol. 187, pp. 291–309, 2003.

[3] F.X. Trias, O. Lehmkuhl, A. Oliva, C.D. Pérez-Segarra and R.W.C.P. Verstappen. Symmetry-preserving discretization of Navier–Stokes equations on collocated unstructured grids. *Journal of Computational Physics*, Vol. 258, pp. 246–267, 2014.

[4] F. Capuano, G. Coppola, H. Gomez and L. de Luca. Energy-preserving Runge–Kutta methods for the incompressible Navier–Stokes equations. *Journal of Computational Physics*, Vol. 298, pp. 480–495, 2015.

[5] B. Sanderse. Energy-conserving Runge–Kutta methods for the incompressible Navier–Stokes equations. *Journal of Computational Physics*, Vol. 233, pp. 100–131, 2013.

[6] E.M.J. Komen, L.H. Camilo, A. Shams, B.J. Geurts and B. Koren. A quantification method for numerical dissipation in quasi-DNS and under-resolved DNS, and effects of numerical dissipation in quasi-DNS and under-resolved DNS of turbulent channel flows. *Journal of Computational Physics*, Vol. 345, pp. 565–595, 2017.

[7] X. Álvarez-Farré, A. Gorobets, F.X. Trias, R. Borrell and G. Oyarzun. HPC^2—A fully-portable, algebra-based framework for heterogeneous computing. Application to CFD. *Computers & Fluids*, Vol. 173, pp. 285–292, 2018.

[8] B. Sanderse and F.X. Trias. Energy-consistent discretization of viscous dissipation with application to natural convection flow. *Computers & Fluids*, Vol. 286, 106473, 2024.

[9] J. Kim, P. Moin and R. Moser. Turbulence statistics in fully developed channel flow at low Reynolds number. *Journal of Fluid Mechanics*, Vol. 177, pp. 133–166, 1987.

[10] F. Nicoud and F. Ducros. Subgrid-scale stress modelling based on the square of the velocity gradient tensor. *Flow, Turbulence and Combustion*, Vol. 62, No. 3, pp. 183–200, 1999.